Comparing the Roles of Barotropic versus Baroclinic Feedbacks in the Atmosphere's Response to Mechanical Forcing

ELIZABETH A. BARNES AND DAVID W. J. THOMPSON

Department of Atmospheric Science, Colorado State University, Fort Collins, Colorado

(Manuscript received 25 February 2013, in final form 1 August 2013)

ABSTRACT

Do barotropic or baroclinic eddy feedbacks dominate the atmospheric circulation response to mechanical forcing?

To address this question, barotropic torques are imposed over a range of latitudes in both an idealized general circulation model (GCM) and a barotropic model. The GCM includes both baroclinic and barotropic feedbacks. The barotropic model is run in two configurations: 1) only barotropic feedbacks are present and 2) a baroclinic-like feedback is added by allowing the stirring region to move with the jet. The relationship between the latitude of the forcing and the response is examined by systematically shifting the torques between the tropics and the pole. The importance of the mean state is investigated by varying the position of the control jet.

Five main findings are presented: 1) Barotropic feedbacks alone are capable of producing the structure of the GCM response to mechanical forcing but are not capable of accounting for its full magnitude. 2) Baroclinic processes generally increase the magnitude of the response but do not strongly influence its structure. 3) For a given forcing, the largest response in all model configurations occurs 5°–10° poleward of the forcing latitude. 4) The maximum response occurs when the forcing is located approximately 10° poleward of the control jet. 5) The circulation response weakens as the mean jet is found at higher latitudes in all model configurations.

1. Introduction

Understanding the extratropical atmospheric response to thermal and mechanical forcing is central to a range of current problems in climate dynamics. Midlatitude atmosphere–ocean interaction is a function of the tropospheric response to variations in surface diabatic heating, stratosphere–troposphere coupling is a function of the tropospheric response to changes in the shear of the flow at the tropopause level and/or diabatic heating in the polar stratosphere, and the circulation response to climate change likely depends in part on the tropospheric response to diabatic heating in the tropical troposphere and at the surface over the Arctic. In all cases, the mechanisms that drive the tropospheric response are not fully understood.

The problem lies not in the balanced response of the extratropical atmosphere to external forcing. The geostrophically and hydrostatically balanced response to thermal and mechanical forcing is both well understood and straightforward to estimate (Haynes and Shepherd 1989; Haynes et al. 1991). Rather, the problem lies in understanding and predicting the subsequent changes in the extratropical eddy fluxes of heat and momentum. For example, most of the forcings above lead to meridional shifts in the ''eddy driven'' jet. The eddy-driven jet is collocated with large eddy fluxes of heat in the lower troposphere and convergence of the eddy-momentum flux at the tropopause level. Thus, understanding and predicting the response of the jet to external forcing can be accomplished only through understanding and predicting the response of its attendant wave fluxes of heat and momentum.

The wave fluxes of momentum are particularly important, as they determine the barotropic component of the flow, project strongly onto the annular modes and their attendant climate impacts, and influence the lower-tropospheric baroclinicity. The response of the wave fluxes of momentum to a given forcing can arise through two sets of processes:

Corresponding author address: Elizabeth A. Barnes, Department of Atmospheric Science, Colorado State University, 1371 Campus Delivery, Fort Collins, CO 80523.
E-mail: eabarnes@atmos.colostate.edu

DOI: 10.1175/JAS-D-13-070.1

© 2014 American Meteorological Society

1) Through changes in the characteristics for meridional wave propagation aloft (i.e., via barotropic processes). For example, changes in the upper-tropospheric mean flow influence the direction of wave propagation into the stratosphere (e.g., Chen and Robinson 1992; Simpson et al. 2009), the phase speed and critical latitudes for meridionally propagating waves (e.g., Chen and Held 2007; Chen et al. 2008), the barotropic stage of the life cycle of baroclinic waves (Wittman et al. 2007), and the geometry of the critical latitudes on the poleward and equatorward flanks of the jet (e.g., Chen and Zurita-Gator 2008; Barnes et al. 2010; Kidston and Vallis 2012).
2) Through changes in the growth of wave activity in the troposphere (i.e., via baroclinic processes). The growth of baroclinic waves is a function of the baroclinicity (e.g., Lindzen and Farrell 1980), and observations reveal robust linkages between variability in the baroclinicity of the flow and the generation of wave activity in the lower troposphere (Thompson and Birner 2012). The linkages between the baroclinicity and wave generation are theorized to play a key role in the dynamics that drive the annular modes (e.g., Robinson 2000; Lorenz and Hartmann 2001) and the extratropical response to stratospheric variability (e.g., Song and Robinson 2004), to extratropical sea surface temperature anomalies (e.g., Brayshaw et al. 2008), and to the thermal forcings associated with climate change (e.g., Kushner et al. 2001; Yin 2005; Frierson et al. 2006; Lu et al. 2008, 2010; O'Gorman 2010; Butler et al. 2011).

The goal of this study is to present a methodology to investigate the relative importance of barotropic and baroclinic eddy feedbacks in determining the structure and amplitude of the extratropical circulation response to mechanical forcing. The study is modeled on the experiments performed in Ring and Plumb (2007, hereafter RP07), in which the dynamical core of a general circulation model is subject to mechanical torques placed over a range of extratropical latitudes. Here we perform similar experiments, but apply a wider range of mechanical forcings to a hierarchy of numerical models with varying representations of extratropical wave–mean flow interactions. As such, the results provide insight into 1) the relationships between the forcing and response latitudes, 2) the relationships between the forcing latitude and climatological-mean jet position, and 3) the physical feedbacks that play a key role in determining the amplitude and structure of the atmospheric response to mechanical forcing. The experiments are described in section 2, results are given in sections 3–5, and discussion and conclusions are given in section 6.

2. Experiments

We conduct a series of experiments similar to those run in RP07, in which the extratropical atmosphere is subjected to a series of mechanical torques centered at a range of latitudes. In all experiments the torque is applied as a tendency in the zonal-mean zonal wind. It is Gaussian in latitude with an e-folding width of $\sim 11°$ (similar to that used in RP07) and maximum amplitude of $1\,\mathrm{m\,s^{-1}\,day^{-1}}$. For each experiment, model integrations are performed with forcing applied at 5° latitude increments between the subtropics and high latitudes.

The relative importance of barotropic and baroclinic processes in determining the circulation response to the imposed mechanical torques is assessed using the following hierarchy of numerical experiments.

1) Experiments run with the full dynamical core of a general circulation model (GCM). The eddy response in the GCM reflects the full suite of (dry) baroclinic and barotropic eddy feedbacks present in the observed atmosphere.
2) Experiments run with a barotropic model in which the latitude of the stirring region (i.e., the source of wave activity) is fixed in time. By construction, the eddy response to a given forcing must be due solely to barotropic eddy feedbacks from wave propagation and dissipation. (See schematic in Fig. 1a.)
3) Experiments run with a barotropic model in which the latitude of the stirring region is in part determined by the strength of the zonal flow. In this case the source of wave activity migrates in response to changes in both the eddy-momentum fluxes (through their influence on the mean winds) and the direct influence of the applied torque on the mean winds. The total eddy response is thus influenced by both barotropic and baroclinic processes. (See schematic in Fig. 1b.)

In this study, we distinguish barotropic feedbacks as those simulated by a barotropic model with fixed stirring (constant eddy source). This definition of barotropic feedbacks thus includes the interaction of the background flow with the wave propagation and dissipation. We note, however, that the barotropic model also includes the influence of the background vorticity gradient on the pseudomomentum source, which can also modulate the eddy fluxes (see Barnes and Garfinkel 2012 for discussion of this feedback). Baroclinic feedbacks are defined as changes in the position and strength of the eddy source due to changes in the low-level baroclinicity. While the GCM inherently includes a suite of barotropic and baroclinic feedbacks that may not be

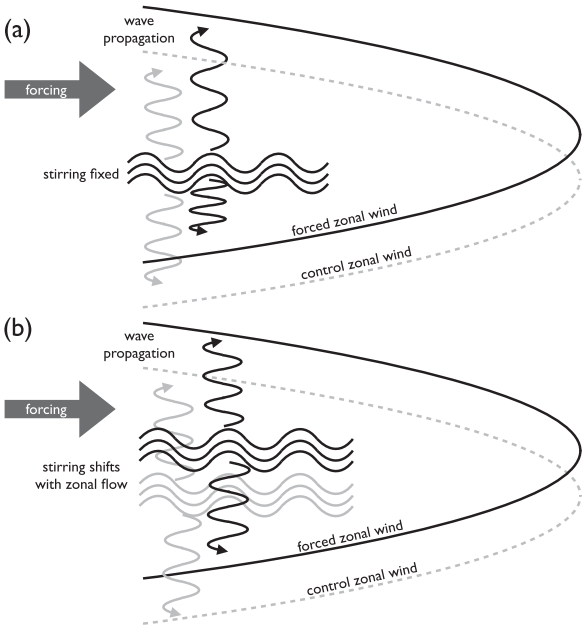

FIG. 1. Schematics of the barotropic model experimental setups: (a) stirring is fixed for the entire run and (b) stirring latitude is partially determined by the latitude of maximum zonal-mean zonal winds. Gray curves denote the control run and the black curves denote the runs forced with an imposed torque poleward of the control jet. Horizontal squiggles denote the stirring region and vertical squiggles denote the eddy wave propagation away from the stirring region.

easily distinguished from one another, the subset of barotropic model experiments that include a baroclinic-like feedback (experiment 3) will only directly simulate the movement of the eddy source (the ''baroclinic zone'') with the movement of the zonal flow. We note, however, that other distinctions between barotropic and baroclinic feedbacks are also possible. For example, baroclinic processes may modulate wave characteristics such as phase speed and wavenumber rather than just the strength and position of the wave generation. We will not be directly simulating these feedbacks in the barotropic model experiments.

Details of all experiment setups are provided below.

a. Experiment 1 setup: GCM

In the GCM experiments we apply the zonal torques to the spectral dry dynamical core used in Held and Suarez (1994). The model parameters are identical to those in Held and Suarez (1994) unless otherwise mentioned. The model is integrated at T42 resolution, with 20 evenly spaced sigma levels and a time step of 1200 s. The model forcing is zonally and hemispherically symmetric. The applied torques are identical at all model pressure levels.

We shift the location of the model control jet as follows. As noted in Simpson et al. (2010) and Garfinkel et al. (2013), modifying the equilibrium temperature profile in the model can meridionally shift the eddy-driven jet without significantly changing the jet speed or the eddy fluxes. Following Garfinkel et al. (2013), the control tropospheric equilibrium temperature profile here is set by the following equation:

$$T_{\mathrm{eq}}(p,\theta) = \max\left[200\,\mathrm{K}, (T_0 - \delta T_{\mathrm{new}})\left(\frac{p}{p_0}\right)^{\kappa}\right], \quad (1)$$

where

$$\delta T_{\mathrm{new}} = \delta T_{\mathrm{HS94}} + A\cos[2(\theta - 45°)]\sin[4(\theta - 45°)] \quad (2)$$

and the control equilibrium tropospheric temperature profile defined by Held and Suarez (1994) is

$$\delta T_{\mathrm{HS94}} = (\Delta T)_y \sin^2(\theta) + (\Delta T)_z \log\left(\frac{p}{p_0}\right)\cos^2\theta. \quad (3)$$

In all simulations, $(\Delta T)_y = 60\,\mathrm{K}$, $(\Delta T)_z = 10\,\mathrm{K}$, $T_0 = 315\,\mathrm{K}$, and all other variables have values defined in Held and Suarez (1994).

The GCM is run under three different control climatologies. The majority of the experiments are run in a configuration that is most like that used in Held and Suarez (1994) [with $A = 0$ in Eq. (2)], and will be referred to as GCM45 experiments since the control jet is located at 45°N. We will investigate the influence of jet location on the response to the torque in two additional experiments in which $A = -2.0$ (GCM43; control jet near 43°N) and $A = +5.0$ (GCM49; control jet near 49°N). Note that the TR2 and TR4 experiments of Simpson et al. (2010) are obtained when $A = -2.0$ and $A = +2.0$.

The zonal-mean zonal-wind field is evaluated in the lower troposphere (875 hPa), since that is where friction acting on the wind field balances the vertically integrated eddy-momentum flux convergence. The eddy-momentum flux convergence is pressure-weighted averaged from 1000 hPa to the top of the atmosphere, where the fluxes are first calculated at each pressure level before the vertical average is applied.

Figure 2a shows the 875-hPa zonal-wind profile for the GCM45 control integration (solid black line). Easterlies exist near the pole and equator, and the westerlies peak near 45°—with this maximum defining the position of the eddy-driven jet. The near-surface westerlies are maintained against drag by the eddies and as evidenced in Fig. 2b, the vertically integrated eddy-momentum flux convergence (EMFC) exhibits a very similar profile to that of the low-level zonal winds. The EMFC maximizes

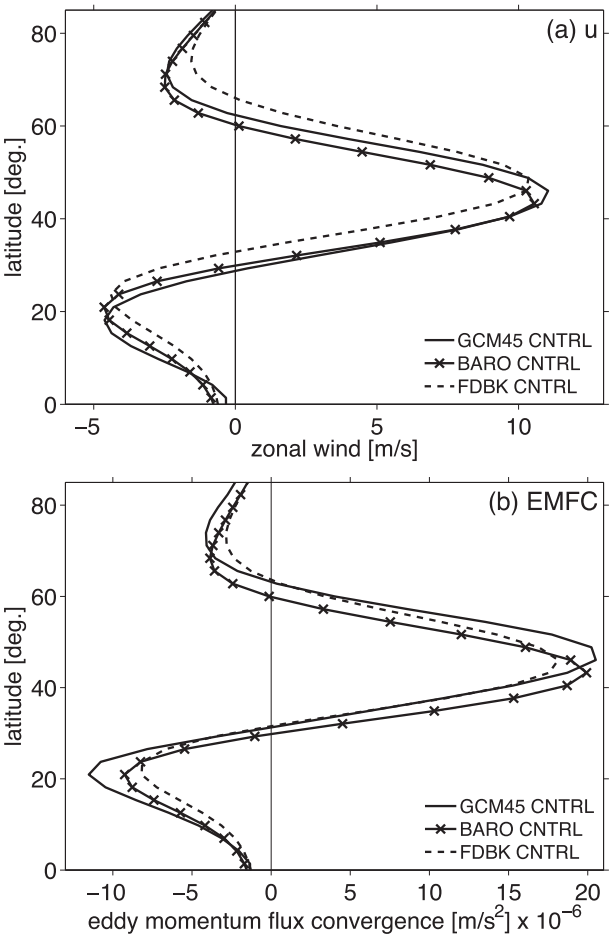

FIG. 2. (a) 875-hPa zonal-mean zonal-wind profiles of the GCM control experiments and the control barotropic model integrations with stirring at 40°. (b) As in (a), but for the vertically integrated eddy-momentum flux convergence.

in midlatitudes and exhibits the largest divergence on the jet flanks where breaking Rossby waves produce an easterly torque.

b. *Experiment 2 setup: Barotropic model with no baroclinic feedback (BARO)*

The goal of the study is to identify the relative roles of barotropic and baroclinic feedbacks in the extratropical atmospheric response to mechanical forcing. To help identify the role of barotropic feedbacks, we analyze output from a stirred barotropic model on the sphere. In the model, stirring of the vorticity parameterizes the wave source. The distribution of the stirring (i.e., strength, shape, and position) remains fixed at all times in the BARO experiments, thus ensuring that the eddy response to the applied torque is solely due to barotropic processes. Details of the model are given in Barnes and Garfinkel (2012) and Vallis et al. (2004), but we discuss key parameters and setup here.

The barotropic model is spectral and nondivergent. Stirring is applied as an additional term in the vorticity tendency equation and is scale specific; stirring occurs over total wavenumbers 8–12, which requires that the zonal wavenumber be greater than 3 in order to emphasize synoptic-scale eddies. The stirring is modeled as a stochastic process, with the vorticity tendency introduced by the stirring ranging between $(-\mathcal{A}, \mathcal{A}) \times 10^{-11}\,\mathrm{s}^{-1}$ and a decorrelation time of 2 days [see Vallis et al. (2004) for additional details].

The stirring is windowed with a Gaussian in physical space (denoted $\mathcal{W}$) in order to produce a meridionally confined storm track. The Gaussian at each time step (t) has a width given by σ_{stir} and is centered on the stirring latitude (θ_{stir}), which is set equal to a fixed latitude (θ_{fixd}) throughout the integration:

$$\mathcal{W}(t,\theta) = \exp[-x(t,\theta)^2], \tag{4}$$

$$x(t,\theta) = \frac{[\theta - \theta_{\mathrm{stir}}]}{\sqrt{2}\sigma_{\mathrm{stir}}}, \quad \text{and} \tag{5}$$

$$\theta_{\mathrm{stir}} = \theta_{\mathrm{fixd}}. \tag{6}$$

In all experiments here, $\sigma_{\mathrm{stir}} = 12°$, which corresponds to a half-width of about 14°. Note that although the stirring shape and position do not vary with the flow, the stirring is wide enough to allow for meridional movement of the jet and the momentum fluxes within the stirring domain. The model is integrated with a time step of 1800 s, and each control run is spun up for 500 days before being integrated an additional 5000 days for analysis. The integrations with an imposed external torque are branched off of the control integration at day 500 and integrated an additional 5000 days.

We will be comparing output from the barotropic and general circulation models to test the relative importance of different eddy feedbacks in the response to identical forcings. For this reason, we wish to limit as much as possible the differences between the model climatologies. To do this, we set the damping time scale, amplitude, and location of the stirring so that two aspects of the climatology in the barotropic model match as closely as possible those from full GCM: 1) the latitude and strength of the maximum zonal-mean zonal wind and 2) the magnitude of the eddy-momentum flux convergence (see Table 1).

The crosses in Fig. 2a show the resulting zonal-mean zonal wind for the control BARO experiment. The crosses in Fig. 2b show the eddy-momentum flux convergences. Here we have used a frictional time scale of 6.5 days, stirring strength of $\mathcal{A} = 9.0$, and a fixed stirring latitude of $\theta_{\mathrm{fixd}} = 40°\mathrm{N}$. The latitude and strength of the

TABLE 1. Summary of mean states in the control simulations. The GCM values are calculated using the 875-hPa winds. Values have been rounded to the nearest 0.2° and 0.5 m s^{-1}.

GCM CNTRL			BARO CNTRL			FDBK CNTRL		
Name	u_{lat} (°)	u_{spd} (m s^{-1})	θ_{fixd}(°)	u_{lat} (°)	u_{spd} (m s^{-1})	θ_{fixd}(°)	u_{lat} (°)	u_{spd} (m s^{-1})
GCM43	42.8	10.5	35	38.0	11.0	35	39.8	10.5
GCM45	45.4	11.0	40	43.6	10.5	40	45.8	10.0
GCM49	49.4	12.0	45	49.2	10.5	45	52.4	10.5
			50	54.7	10.5	50	57.2	11.0
			55	59.0	11.0	55	60.6	11.0

maximum zonal-mean zonal winds agree well with that of the GCM by construction (Fig. 2a). However, the wind profiles themselves are determined purely by the eddy fluxes in each model (i.e., the internal dynamics of the flow). The agreement between the climatological-mean zonal flow of the GCM and barotropic model attest to the utility of the barotropic model for simulating that part of the GCM zonal wind that is driven by eddy-momentum fluxes.

c. *Experiment setup 3: Barotropic model with baroclinic feedback (FDBK)*

In the BARO experiment setup described above, the stirring latitude remains fixed throughout the entire integration. Hence, meridional shifts in the momentum fluxes and zonal jet do not influence the location of the stirring. In the FDBK experiment setup, we use the same barotropic model and setup as in BARO, except here the latitude of the stirring is determined in part by the zonal-mean zonal flow. Specifically, a meridionally confined storm track is created from the global stirring by windowing the gridded stirring field with a spatial mask $\mathcal{W}$ as in the BARO experiments. The quantities $\mathcal{W}$ and x are defined as in Eqs. (4) and (5), but in this case

$$\theta_{\text{stir}}(t) = \frac{1}{2}[(1-\alpha_{\text{fdbk}})\theta_{\text{fixd}} + \alpha_{\text{fdbk}}\theta_{\text{jet}}(t)], \qquad (7)$$

where $\theta_{\text{jet}}(t)$ is the latitude of the maximum zonal-mean zonal winds at time step t and is calculated during model integration at each time step. In this way, θ_{stir} moves with the jet to simulate the linkages between the zonal-mean upper-level flow and lower-level baroclinicity (i.e., since the zonal flow goes to zero at the surface, the vertical shear of the flow is proportional to the flow at upper levels). The location of the stirring is thus given in part by θ_{fixd}, which can be viewed as reflecting the influence on baroclinicity of forcings that are fixed in time (e.g., meridional gradients in radiation, ocean currents, etc.), and θ_{jet}, which can be viewed as reflecting the influence on baroclinicity of both the momentum fluxes and the torque.

The strength of the baroclinic-like feedback is set by α_{fdbk}, which is a value between 0 and 1. Note that when $\alpha_{\text{fdbk}} = 0$, there is no feedback between the zonal flow and the latitude of the stirring regions, and the stirring is identical to that in the BARO experiment. The feedbacks are introduced on day 500 of the control BARO experiment to allow the jet and eddies to come into equilibrium without the baroclinic feedback present and then spun up an additional 500 days before the 5000-day integration.

The amplitude of α_{fdbk} was chosen as follows. Figures 3a,b show histograms of the daily latitude of θ_{jet} (solid black lines) and θ_{emfc} (the latitude of the maximum eddy-momentum flux convergence; dashed black lines) for the control (unforced) GCM45 and BARO runs. Both the GCM and the barotropic model show distributions of jet latitude that are narrower than the distributions of the eddy-momentum flux convergence; highlighting that the maximum eddy forcing on daily time scales does not always align with the zonal jet. This is possible when the zonal-wind acceleration due to the shifted eddy forcing is not enough to shift the zonal-wind maximum. Note, however, that the eddy-momentum flux convergence and the surface winds must balance in steady state.

Careful comparison of Figs. 3a and 3b demonstrates that the widths of the distributions of θ_{jet} and θ_{emfc} are larger in GCM45 than in BARO, implying that the jet and eddies can move farther away from their time-mean locations in the GCM. Table 2 shows that this is the case, where the standard deviations of θ_{jet} is 4.0° in the GCM, but 3.0° in BARO and the standard deviation of θ_{emfc} is 1.0° larger in the GCM.

We run five different FDBK control experiments, where α_{fdbk} varies between 0.25 and 0.75. The histograms are shown in Figs. 3c–f and the corresponding spreads are given in Table 2. As the feedback is increased in the barotropic model (α_{fdbk} increases), the standard deviation of θ_{jet} and θ_{emfc} increases as well, demonstrating that increasing the feedback parameter allows the eddies and the eddy-driven jet to shift further from θ_{fixd} on any given day.

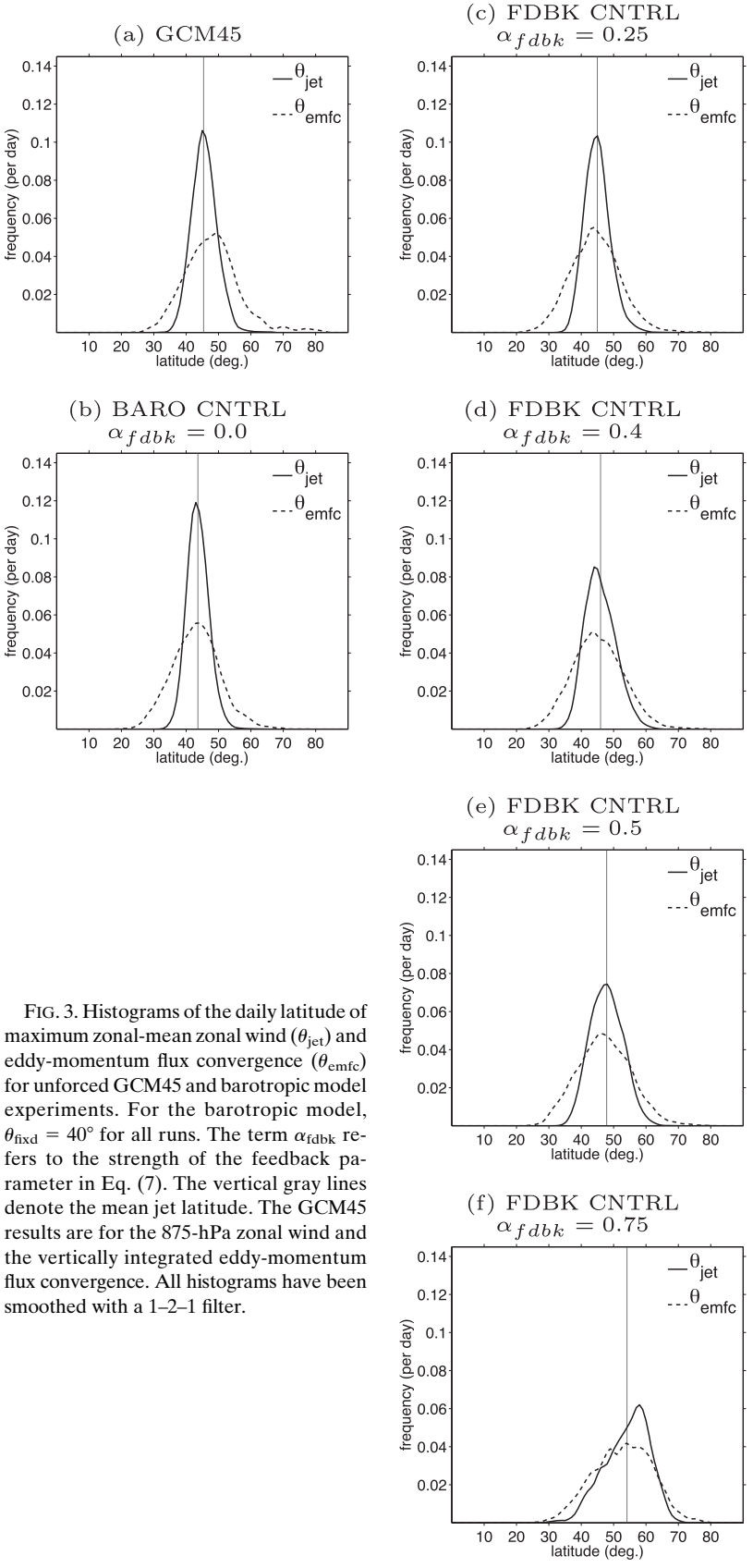

FIG. 3. Histograms of the daily latitude of maximum zonal-mean zonal wind (θ_{jet}) and eddy-momentum flux convergence (θ_{emfc}) for unforced GCM45 and barotropic model experiments. For the barotropic model, $\theta_{\text{fixd}} = 40°$ for all runs. The term α_{fdbk} refers to the strength of the feedback parameter in Eq. (7). The vertical gray lines denote the mean jet latitude. The GCM45 results are for the 875-hPa zonal wind and the vertically integrated eddy-momentum flux convergence. All histograms have been smoothed with a 1–2–1 filter.

TABLE 2. Standard deviation of the daily latitude of the maximum zonal-mean zonal winds (σ_{jet}) and zonal-mean eddy-momentum flux convergence (σ_{emfc}) for unforced GCM45 and barotropic model experiments. For the barotropic model experiments, θ_{fixd} = 40° for all runs. The term α_{fdbk} refers to the strength of the feedback. The GCM45 results are for the 875-hPa zonal wind and the vertically integrated eddy-momentum flux convergence. Values have been rounded to the nearest 0.5°.

Control experiment	$\sigma_{\theta_{jet}}$ (°)	$\sigma_{\theta_{emfc}}$ (°)
GCM45	4.0	8.5
BARO		
α_{fdbk} = 0.00	3.0	7.5
FDBK		
α_{fdbk} = 0.25	4.0	7.5
α_{fdbk} = 0.40	4.5	8.0
α_{fdbk} = 0.50	5.0	8.5
α_{fdbk} = 0.75	7.0	9.0

For α_{fdbk} = 0.25, the mean jet position (vertical lines in Fig. 3) remains near 45°N, similar to the BARO and GCM45 experiments. However, for $\alpha_{fdbk} \geq 0.4$, the jet and EMFC distributions shift poleward. This propensity for the eddies and jet to migrate poleward is likely due to the mechanism first explored Feldstein and Lee (1998), where the preference for waves to propagate and break on the equatorward flank of the jet causes the jet and eddies to shift poleward over time.

For the subsequent analysis, we have chosen to set the feedback parameter α_{fdbk} = 0.4. An α_{fdbk} of 0.4 gives the largest agreement between the GCM response and the barotropic model response (quantified by the spatial covariance of the responses to be discussed in section 4). In addition, an α_{fdbk} of 0.4 gives an *e*-folding time scale (τ) of the FDBK control annular-mode time series (the annular mode is defined as the leading EOF of the zonal-mean zonal wind) of approximately 13 days. This value compares reasonably well with the observed *e*-folding time scale of the tropospheric southern annular mode (Gerber et al. 2008). We note, however, that while the FDBK control experiment with α_{fdbk} = 0.4 gives a reasonable annular-mode time scale, the GCM substantially overestimates this time scale by a factor of 2 (36 days). This bias in the GCM toward long time scales is well documented and appears to be sensitive to model resolution, topography, and mean state (Gerber and Vallis 2007; Wang et al. 2012). Annular-mode time scales for the BARO and FDBK runs with varying feedback strengths are given in Table 3, and the persistence of the annular mode increases with increasing feedback strength.

The primary results in the next section were also tested for α_{fdbk} = 0.25 and 0.5. The findings for these additional experiments are presented in appendix A. The magnitude of the response changes as the feedback changes, but the results are otherwise qualitatively similar.

TABLE 3. Annular-mode *e*-folding time scales (τ) for the GCM and barotropic model integrations where θ_{fixd} = 40°N and α_{fdbk} refers to the strength of the feedback parameter in Eq. (7).

GCM CNTRL		BARO and FDBK CNTRL	
	τ (days)	α_{fdbk}	τ (days)
GCM43	41	0.00	6
GCM45	36	0.25	9
GCM49	20	0.40	13
		0.50	13
		0.75	22

3. The GCM response to an external torque

We will first discuss the circulation response in the GCM45 experiments. By construction, the response includes the full suite of (dry) baroclinic and barotropic feedbacks. We will then compare the full GCM responses to those derived from the barotropic model experiments with different representations of the eddy feedbacks.

Figure 4 shows the zonal-mean near-surface zonal-wind response in the GCM45 experiments. The format used to construct Fig. 4 will be used throughout the study. The abscissa denotes the latitude at which the forcing is centered, the ordinate is used to denote the latitude of the response, and the dotted black line denotes the

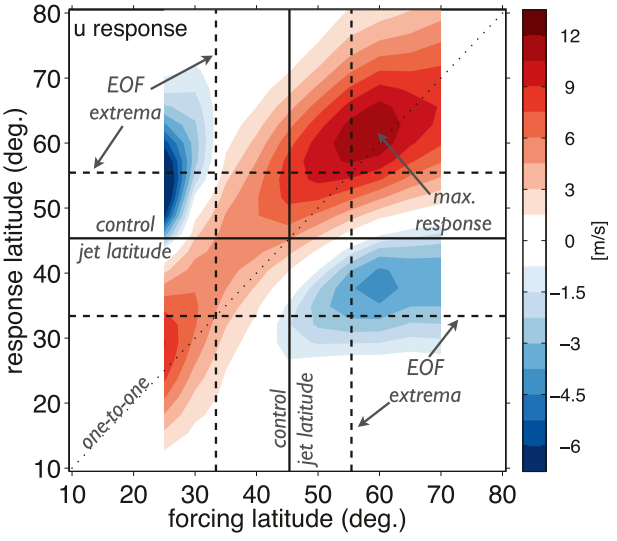

FIG. 4. GCM45 experiment results for imposed barotropic torques. Plotted is the response of the 875-hPa zonal winds. Also plotted are the control jet latitude position (solid lines), zonal-wind EOF1 extrema (dashed lines), and the one-to-one line (dotted line).

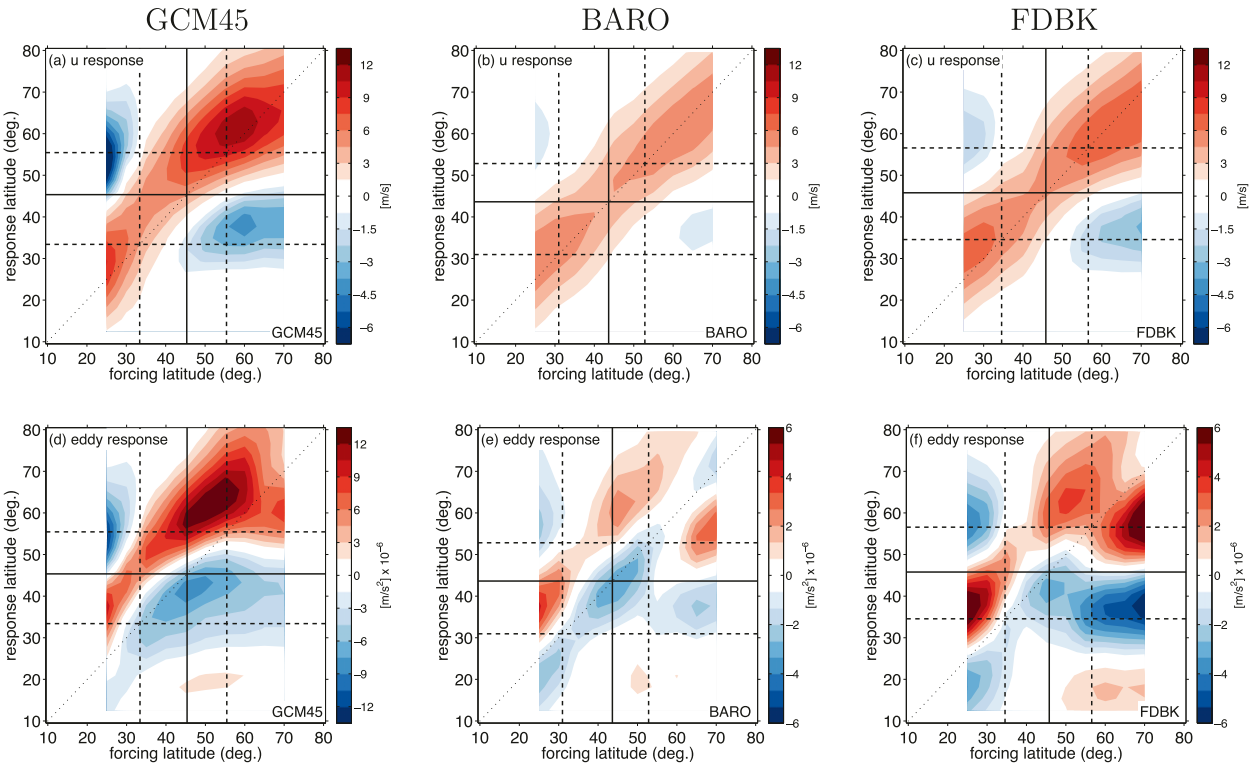

FIG. 5. Response of (a)–(c) the zonal-mean zonal winds and (d)–(f) eddy-momentum flux convergence for imposed barotropic torques. Each column refers to a different model experiment. All other lines are as in Fig. 4. Note the different scales in (d)–(f).

one-to-one line (i.e., if the response occurred at the same latitude as the forcing, it would lie along the one-to-one line). The thick solid lines denote the position of the control jet and the dashed lines denote the centers of action of the model annular mode in the zonal-mean zonal wind. In the GCM45 simulations, the control jet lies at 45.4°N and the centers of action of the annular modes at 35.4° and 54.5°N. The forcing is applied between 25° and 70°N in increments of 5°. We do not apply the forcing equatorward of 25°N since the momentum balance in the GCM and barotropic model differ significantly there, with the GCM exhibiting a Hadley circulation, which the barotropic model cannot simulate.

Before we consider the responses in Fig. 4, it is useful to consider the response that would result in the absence of eddy feedbacks. At steady state the vertically integrated zonal-mean momentum equation can be approximated as

$$0 = \left\langle \frac{\partial(u'v')}{\partial y} \right\rangle - \frac{u_{\rm sfc}}{\tau_f} + \mathcal{F}_{\rm torque}, \tag{8}$$

where $\mathcal{F}_{\rm torque}$ denotes the external momentum forcing, $u_{\rm sfc}$ denotes the boundary layer wind, τ_f denotes the frictional damping time scale, and angle brackets denote the vertical integral. If the eddy fluxes are unchanged, then the torque is balanced by friction and

$$\mathcal{F}_{\rm torque}\tau_f \sim u_{\rm sfc}. \tag{9}$$

Hence, in the absence of eddy feedbacks, the zonal-wind response in Fig. 4 would be organized along the one-to-one line with the same amplitude at all latitudes. [This can be seen in Fig. 8a where we show that the zonal-mean zonal-wind response lies along the forcing axis in the barotropic model with no eddies ($\mathcal{A} = 0$).] Clearly, this is not the shape of the response in Fig. 4. Consistent with RP07, the response peaks not when the forcing is applied at the axis of the jet (45°) but when it is applied on the jet flank (55°). The easterly wind anomalies in the figure are the hallmark of the eddy forcing, as discussed below.

The results in Fig. 4 are reproduced in Fig. 5a. Figure 5d shows the corresponding changes in the eddy-momentum flux convergence. The most robust aspect of the GCM eddy response is that the imposed torque leads to changes in the eddy fluxes of momentum, regardless of the latitude of the forcing. Beyond this, the response can be divided into two regimes:

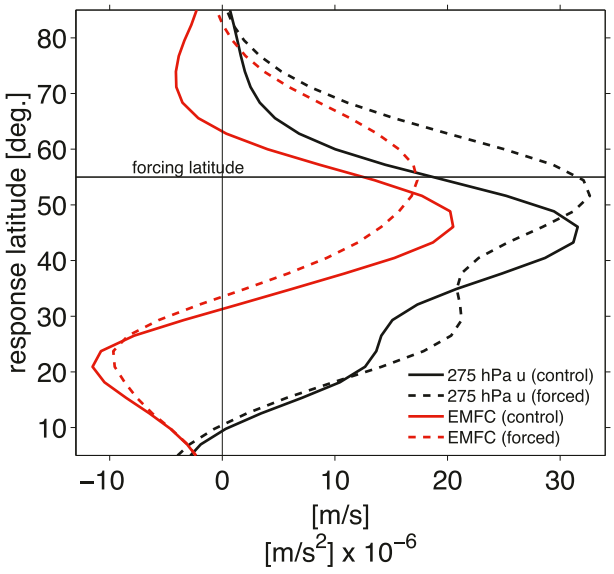

FIG. 6. Example of the 275-hPa zonal-mean zonal winds for the GCM45 control integration (solid black line) and for when a torque is imposed at 55°N (dashed black line). Also plotted are the vertically integrated eddy-momentum flux convergence profiles for the control integration (solid red line) and forced integration (dashed red line).

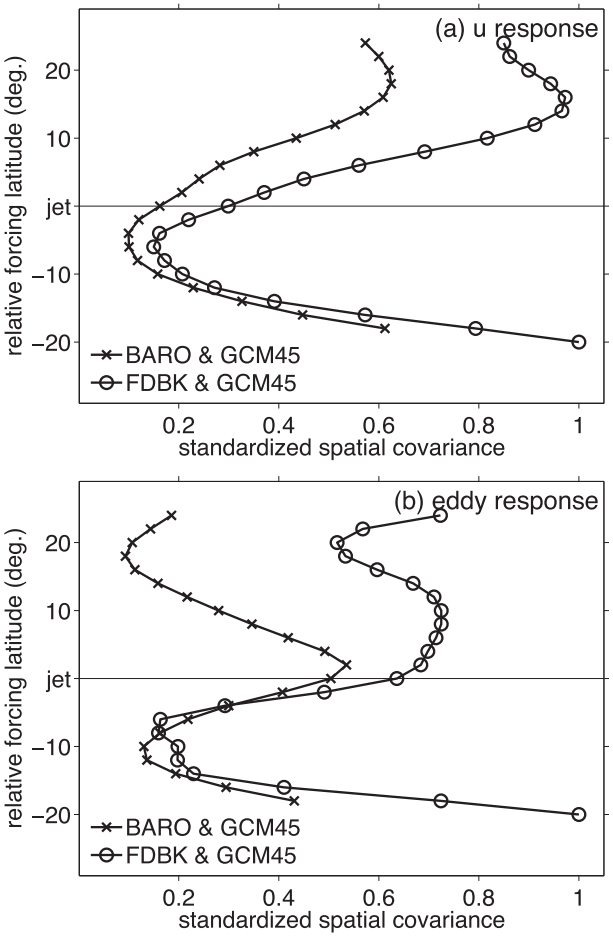

FIG. 7. Spatial covariance between the GCM45 and barotropic model (a) zonal-wind and (b) eddy responses (refer to Fig. 5) as a function of the distance of the forcing from each integration's control jet position. The covariance is calculated between 10° and 80°N and scaled with arbitrary units for plotting.

1) When the torque is applied between latitudes 25° and 60°N, the eddy response is marked by anomalous eddy-momentum flux convergence on the poleward side of the forcing and anomalous eddy-momentum flux divergence on the equatorward side of the forcing. The eddies thus act to shift the zonal winds poleward of where they would equilibrate with the torque alone.
2) When the torque is applied poleward of 60°N, the anomalous eddy-momentum flux convergence maximum is located south of the torque.

The results in Fig. 5d confirm that the eddy response to mechanical forcing is largest when the forcing is applied on the jet flank, but they also reveal that regardless of the forcing latitude, the maximum zonal-wind response lies roughly 5°–10° poleward of the torque. For example, when the forcing coincides with the poleward center of the model annular mode (55°N), the response itself peaks near 65°N.

That the eddy response lies poleward of the forcing latitude is consistent with the nature of meridionally propagating waves. In regions where the flow already permits a range of phase speeds, increases in the flow have little effect on the range of phase speeds that are permitted there. In contrast, in regions where the flow is relatively weak, incremental changes in the zonal flow have a much larger effect on the range of phase speeds permitted there. The changes in the wave forcing should thus peak on the flanks of the jet, where the flow is relatively weak, thus shifting the jet poleward (or equatorward, in the case of a low-latitude torque).

For example, consider Fig. 6, where we plot the upper-level (275 hPa) zonal-mean zonal winds for the GCM45 control (solid black curve) and the integration with an imposed torque at 55°N (dashed black curve). The red curves denote the total eddy-momentum flux convergence profiles for each integration. The winds increase by 14 m s^{-1} at the latitude of the forcing (from ~18 to 32 m s^{-1}) and 6 m s^{-1} on the flank of the jet at 70°N (from ~4 to 10 m s^{-1}). The increase in wind speed is larger at the latitude of the forcing, but has a relatively small effect on the phase speeds permitted there since 1) waves with phase speeds <18 m s^{-1} account for the

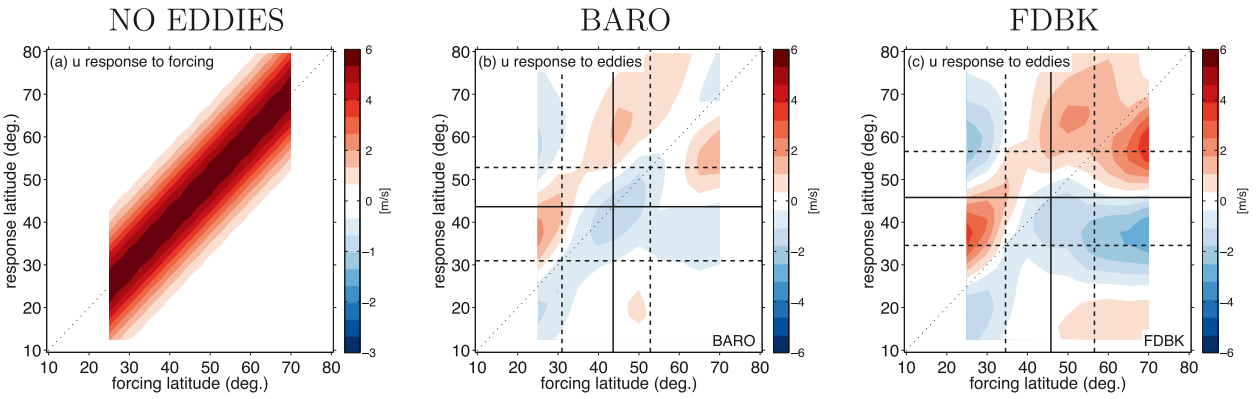

FIG. 8. As in Fig. 5, but displaying the barotropic model wind response due solely to (a) the forcing alone (no eddies) and (b),(c) the eddies.

majority of the momentum fluxes in the extratropics and 2) waves with phase speeds from 0–18 m s^{-1} were already permitted at the latitude of the forcing. It follows that the relatively small increase in the flow from 4 to 10 m s^{-1} at 70°N has a more pronounced effect on the permitted wave fluxes.

Figures 5a,d demonstrate that the eddies induce a dipolar response in the winds for forcing on the flanks of the control jet. When the torque is applied at the latitude of the control jet, the zonal-wind response is weak since the eddies oppose the torque there; that is, there is anomalous divergence at the torque latitude. Similar conclusions were reached in RP07, but our inclusion of forcings across a wider range of latitudes yields the following additional insights into the GCM response to mechanical forcing:

1) For each forcing latitude, the maximum wind and eddy response lies 5°–10° poleward of the forcing. The eddies thus act to shift the zonal winds poleward of where they would equilibrate with the torque in the absence of eddy feedbacks.
2) The circulation response is largest when the torque is applied approximately 10° poleward of the control jet latitude. (Again, the maximum response is found 5°–10° poleward of the torque.)

RP07 suggest that the maximum wind response occurs when the torque projects onto the centers of action of the annular mode in the wind field. We find a similar result for GCM45 but for two key additional findings: 1) consistent with insight 1 above, the maximum response is shifted poleward of the annular-mode maximum and 2) as we note in section 5, the response is sensitive to the climatological-mean state of the flow.

Since part of the motivation for this work is to extend the results of RP07, appendix B presents additional GCM simulations using parameters similar to those used in RP07.

4. Barotropic versus baroclinic feedbacks

The response of the GCM to mechanical forcing includes both (dry) barotropic and baroclinic eddy feedbacks. In this section we will use the BARO and FDBK configurations to estimate the relative importance of each feedback process in the circulation response. The middle and right columns of Fig. 5 show the results from the barotropic model experiments: the barotropic case (BARO; middle) and the case where the eddy source moves with the peak in the zonal-mean zonal winds (FDBK; right). The wind responses in both barotropic model configurations are dominated by accelerated winds along the torque axis, with the weakest responses found when the forcing is near the control jet latitude (as is true for the GCM). Both experiments also exhibit dipolar responses in the winds when the forcing is placed on the flanks of the jet. In all cases, the wind responses are weaker in the runs without the baroclinic eddy feedback.

The eddy responses can be divided into two regimes: 1) the forcing is located south of ~60°N and the barotropic eddy feedbacks act against the torque over a latitude band centered around the forcing and support the torque poleward of the forcing (Fig. 5e) and 2) the forcing is located poleward of ~60°N and the eddy response is restricted to latitudes equatorward of the forcing. In the case of regime 1, the barotropic eddy feedbacks act against the torque for forcing near the jet latitude (blue shading near 45°N in Fig. 5e), consistent with the findings of Barnes and Garfinkel (2012) where they demonstrated that barotropic eddies oppose external forcing on the mean flow at the latitude of the forcing.

The eddy responses in the GCM45, BARO, and FDBK experiments exhibit several similarities. In all configurations, forcings located equatorward of ~60°N are associated with eddy-momentum flux convergence poleward of the forcing and eddy-momentum flux

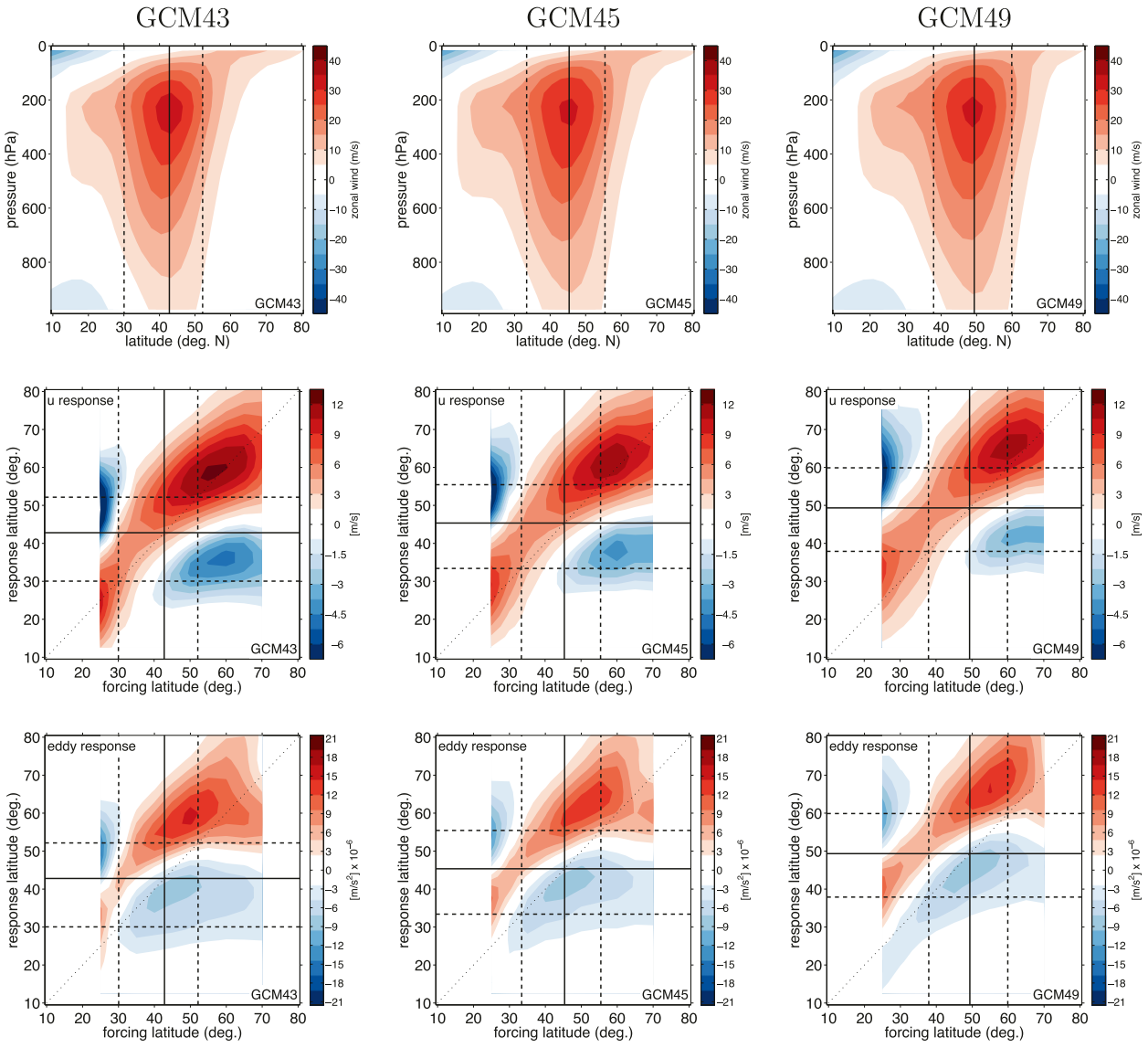

FIG. 9. As in Fig. 5, but for the three GCM experiments only and with (top) the vertical structure of the zonal-mean zonal winds for each model setup.

divergence equatorward of the forcing. Forcings located poleward of ~60°N are associated with eddy-momentum flux convergence and divergence anomalies that are both centered equatorward of the forcing. The primary difference between BARO and FDBK lies in the magnitude of the responses: in general the eddy response is 50% larger in the FDBK configuration. For the most part, it appears that barotropic dynamics may play a key role in setting the structure of the response in the GCM, while baroclinic feedbacks set the amplitude. Note that both GCM45 and FDBK show local maxima in the eddy response when the forcing is placed near the EOF maximum and similarities between the GCM and FDBK wind responses are also notable in this region. On the other hand, BARO exhibits a local eddy response maximum when the forcing is placed just poleward of the jet latitude, and this is not found in the GCM or FDBK results.

Figure 7 quantifies the similarities and differences between 1) the GCM45 response and 2) the responses of the two barotropic model configurations. The figure shows the spatial covariance of the responses between 10° and 80°N. The response fields are first interpolated to a 0.5° grid, and then the response profiles for different forcing positions are projected onto each other as a function of the distance of the forcing from the control jet. This is done to account for differences in the mean

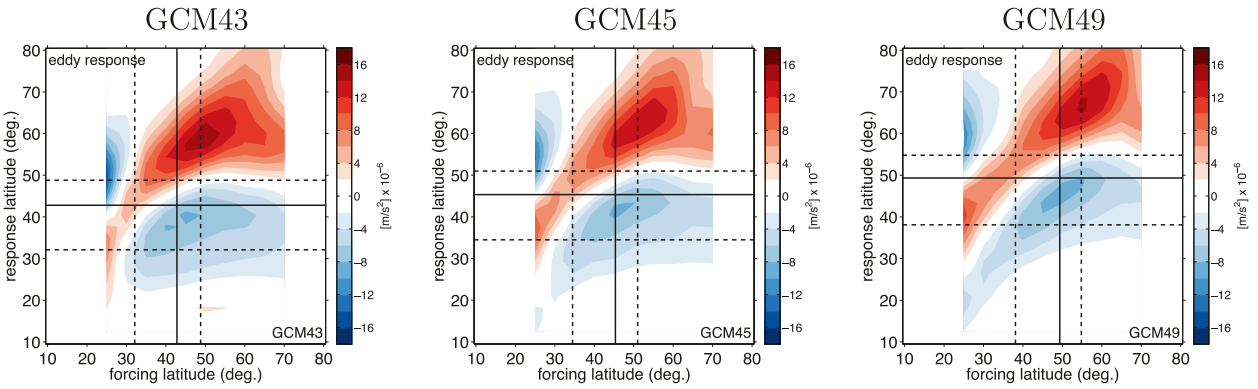

FIG. 10. As in the bottom row of Fig. 9, but the dashed lines denote the eddy-momentum flux convergence EOF1 extrema.

states of the various model configurations. The covariance (rather than correlation) is chosen so as to take into account both the pattern and magnitude of the responses, and the values are scaled so that the largest agreement is equal to 1.

Figure 7a reveals that the addition of a baroclinic-like feedback to the barotropic model acts to noticeably improve the zonal-wind response similarities with the full GCM response. The improvement is evident for all forcing latitudes. The agreement between the zonal-wind responses for both BARO and FDBK and the GCM response are largest for forcing on the flanks of the control jet and smallest for forcing about 5° south of the control jet.

Figure 7b shows the associated spatial covariances of the eddy responses (Figs. 5d–f). Again, for forcing on the flanks of the jet, the FDBK experiment provides better agreement with the GCM than the BARO experiment. And again, the agreement with the GCM is lowest just south of the control jet latitude for both experiments. In general, the FDBK experiment does a better job than BARO for forcings applied poleward of the jet and similarly for forcings applied equatorward. The weak agreements between the GCM and FDBK responses are visually apparent in Figs. 5d,f, where FDBK exhibits little response for forcing 10° south of the jet.

Thus, the FDBK results suggest that a key to simulating the GCM response for forcing away from the jet is allowing the stirring region, and thus the baroclinic zone, to move with the circulation. Comparing BARO with FDBK in Figs. 5e,f, barotropic feedbacks appear to explain approximately two-thirds of the FDBK response, leaving the other one-third to be explained by baroclinic-like feedbacks.

Finally, we quantify the magnitude of the wind response due solely to the eddies in the barotropic experiments. In the barotropic model, the control winds are purely eddy driven, allowing the direct response of the zonal winds to the torque to be computed. As shown in Eq. (9) and Fig. 8a, we can empirically determine the response of the winds due purely to the torque by running additional barotropic model experiments without eddies (where $\mathcal{A} = 0$). We have performed such integrations, and find that the maximum wind response is approximately $6.0\,\mathrm{m\,s^{-1}}$ (refer to Fig. 8a). Equation (9) predicts a maximum of $6.5\,\mathrm{m\,s^{-1}}$, but neglects the higher-order diffusion term in the model that removes enstrophy at small scales, resulting in a slightly weaker wind response.

By subtracting $\overline{u}$ (Fig. 8a) from the total zonal-mean zonal-wind response of the forced integrations with eddies (Figs. 5b,c), one can calculate the indirect response of the winds to the torque via eddy feedbacks alone (Figs. 8b,c). Note that since the torque is zonally symmetric and thus applied only to the zonal-mean budget, the eddy response is brought about solely by changes in the zonal-mean winds and thus signifies either a barotropic or baroclinic-like eddy-mean flow feedback. As expected, eddy feedbacks explain all of the wind response away from the torque latitude. For forcing near the jet center, the eddies generally oppose the torque.

5. Dependence of the response on the mean state

In this section, we investigate the role of the mean state on the response of the circulation to an external torque. We perform this analysis based upon the recent results of Garfinkel et al. (2013) and Simpson et al. (2010, 2012), where the magnitude of the tropospheric jet response to stratospheric forcing decreases as the mean jet is located farther from the equator. Consistent with those studies, Barnes and Hartmann (2011) and Barnes and Polvani (2013) demonstrate that the meridional shifts in the flow associated with the annular

mode varies across a range of models as a function of the mean jet latitude, with higher-latitude jets experiencing smaller shifts in the flow, and vice versa. By modifying the equilibrium temperature gradient to move the tropospheric jet (refer to section 2), we can investigate to what degree the response magnitude to the same mechanical torque is a function of the mean jet latitude. We will show that the latitude of the jet appears to play a role in modulating the response and that this effect is present in the barotropic model runs.

a. Varying the mean state in the GCM

Figure 9 displays results for the three GCM configurations outlined in section 2, with the GCM45 experiment repeated for comparison. The jet latitude and jet speed for each run are summarized in Table 1. The vertical structure of the zonal-mean zonal winds is shown in the top rows of Fig. 9, with the black vertical line denoting the mean jet latitude. The second and third rows of Fig. 9 display the response of the 875-hPa winds and the vertically integrated EMFC to the applied torques (as in Fig. 5). Many of the features previously described for the GCM45 experiment are also present in the GCM43 and GCM49 configurations and so will not be discussed here. What is of interest to us are the differences in the responses between the three simulations.

Comparison of the responses in Fig. 9 shows that contrary to the results of RP07, the wind and eddy responses are not always maximized for forcing at the zonal-wind EOF latitude (dashed lines). For example, in GCM43 the maximum wind response occurs for forcing poleward of the zonal-wind EOF maximum, near 55°N; in GCM49, the maximum eddy response occurs for forcing equatorward of the EOF maximum, again near 55°N. The maximum eddy response does align remarkably well with the EOFs of the eddy-momentum flux convergence, as shown by the dashed lines in Fig. 10. With this in mind, one would not necessarily expect the wind response to align with the zonal-wind EOF, as the wind response is a function of both the eddy response and the direct forcing by the torque. Hence, the pattern of variability in the EMFC may be a better indicator of the structure of the circulation response to external forcing, at least on the poleward flank of the jet.

In the rest of this section we will focus on the weakening of the wind and eddy responses to the torque in Fig. 9 as the jet moves poleward. A dependence on latitude of the tropospheric response to stratospheric perturbations was found by Garfinkel et al. (2013) and Simpson et al. (2010, 2012) and Fig. 9 shows a reduced wind and eddy response going from GCM43 to GCM45 to GCM49. A weakening of the eddy response can be brought about in two ways (or a combination of the two): 1) a decrease in the difference between the magnitude of the forced and control EMFC while the structure of the EMFC remains fixed or 2) a decrease in the shift of the EMFC while the magnitude of the EMFC remains fixed. We cannot comment on the former since the control EMFC profiles differ by approximately 10% among the configurations (although the largest control EMFC corresponds to the configuration with the smallest response). We do, however, find evidence of the latter—that is, that the eddy fluxes shift less for higher-latitude jets. This is evident in Fig. 11a, which displays the time-mean EMFC profiles of the integrations where

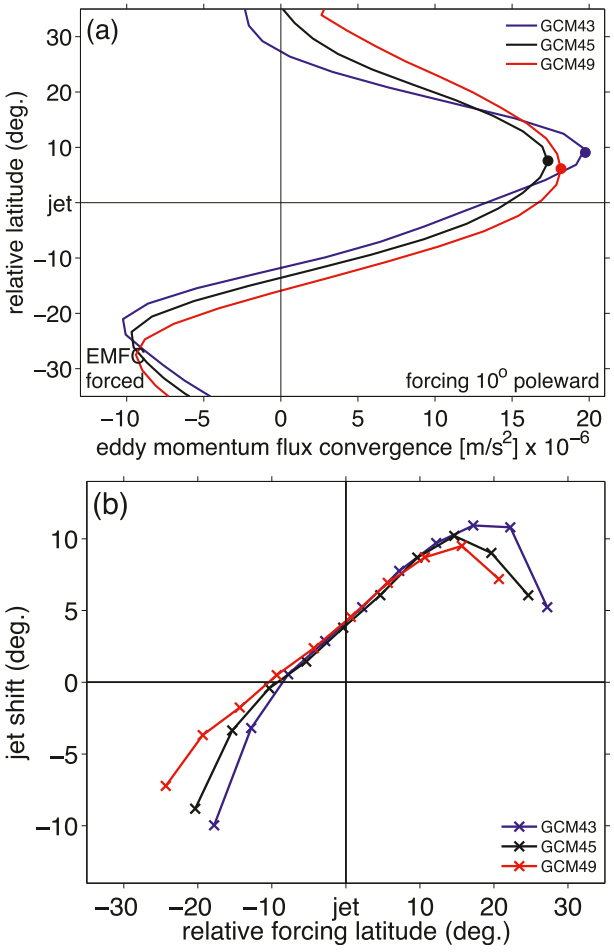

FIG. 11. (a) Total eddy-momentum flux convergence for forced GCM runs when the torque is applied approximately 10° poleward of the jet. The curves are plotted as a function of relative latitude, defined as the distance from the control jet latitude for each GCM configuration. (b) The shift of the jet (latitude of maximum zonal-mean zonal winds) vs the relative forcing latitude (distance from the control jet latitude) in the three GCM experiments.

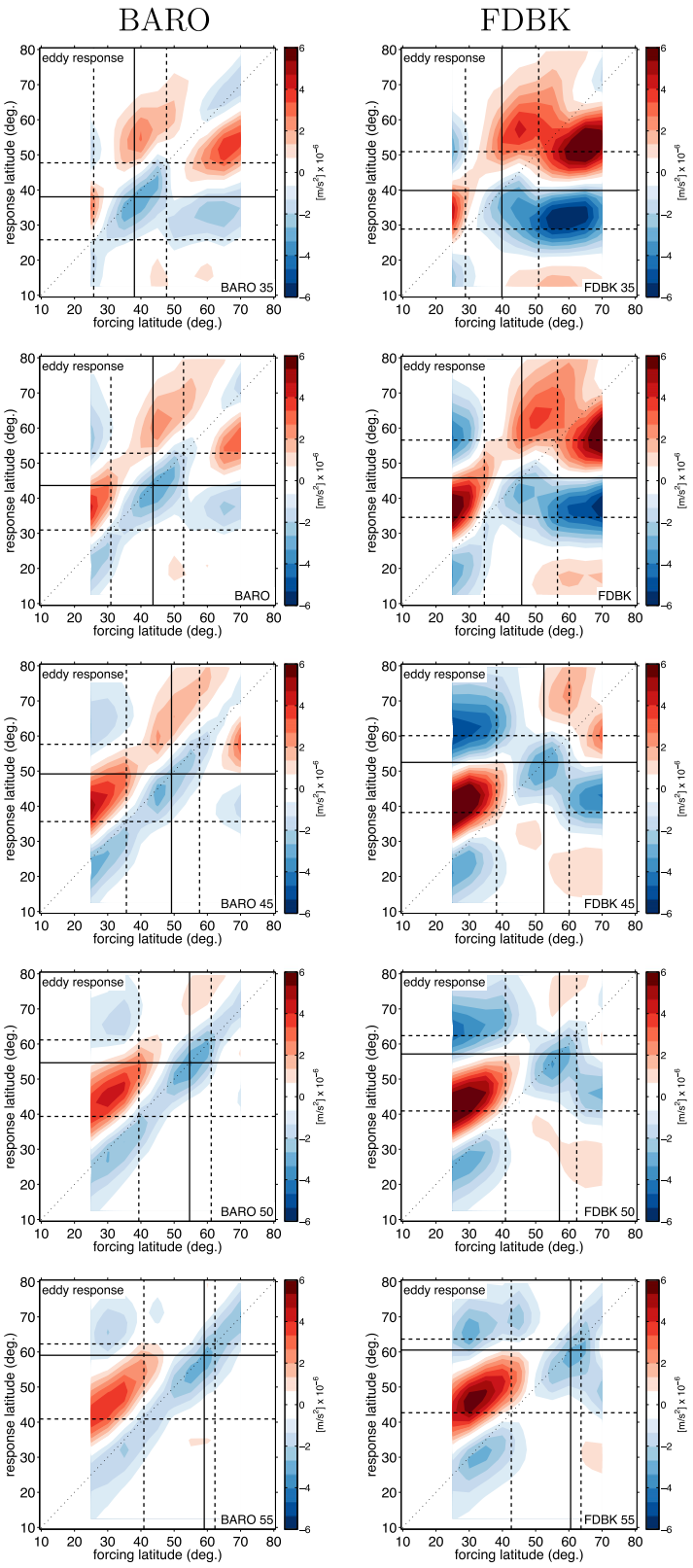

FIG. 12. The eddy response from the barotropic model experiments (left) BARO and (right) FDBK for varying mean states. Stirring latitude (and thus jet latitude) increases from (top) to (bottom), with the θ_{fixd} denoted in the bottom right corner of each panel.

the torque is applied 10° poleward of the control jet latitude. The amount of shift is the distance between the peak EMFC and the zero line. Going from the lowest-latitude jet to the highest (blue curve, black curve, red curve), the amount that the eddy fluxes shift with the forcing decreases.

The differences in eddy responses among the three GCM experiments feed back on the mean flow, and Fig. 11b shows that the jet shifts most when the EMFC response shifts most (lower-latitude jets). For GCM43, the jet can shift as far as 11° from its control latitude, while GCM49 shifts a maximum of 9°. These results are consistent with those of Garfinkel et al. (2013) and Simpson et al. (2010, 2012), where higher-latitude jets shift less in response to the same forcing. In addition, Table 3 confirms that the annular-mode time scales in the GCM experiments decrease as the control jet is located at higher latitudes, suggestive of a weaker eddy–mean flow feedback.

Note that unlike the model setup of Garfinkel et al. (2013) (which has a well-resolved stratosphere), the subtropical jet in our GCM simulations is very weak (as in Simpson et al. 2010). Thus, although Garfinkel et al. (2013) and Barnes and Hartmann (2011) show that the circulation may also be less sensitive to a mechanical forcing for low-latitude jets in the presence of strong subtropical winds, our results do not directly conflict with their results owing to the weak subtropical jet in our simulations and the fact that the midlatitude jet is never located south of 40° latitude in these experiments.

b. Varying the mean state in the barotropic model

The GCM results point to a potential latitudinal constraint on the response of the circulation to a mechanical torque, and we next present a similar dependence on the mean state in the barotropic model. Figure 12 displays the EMFC response for the barotropic experiments (columns) with θ_{fixd} varying every 5° between 35° and 55°N (rows). The jet wind speeds and EMFC magnitudes are similar among all control runs (not shown), and so comparisons of response magnitudes are justified. As the jet is formed at higher latitudes, the EMFC response poleward of the high-latitude forcing decreases. This is the case for FDBK (the integrations most like the GCM) but also for the BARO experiment, where only barotropic feedbacks are present. For the highest-latitude jet ($\theta_{\text{fixd}} = 55°$), the eddy responses appear very similar between FDBK and BARO. This suggests that for high-latitude jets, the baroclinic feedbacks (shifts of the wave source) contribute less to the total eddy response, with barotropic feedbacks explaining the majority of the response.

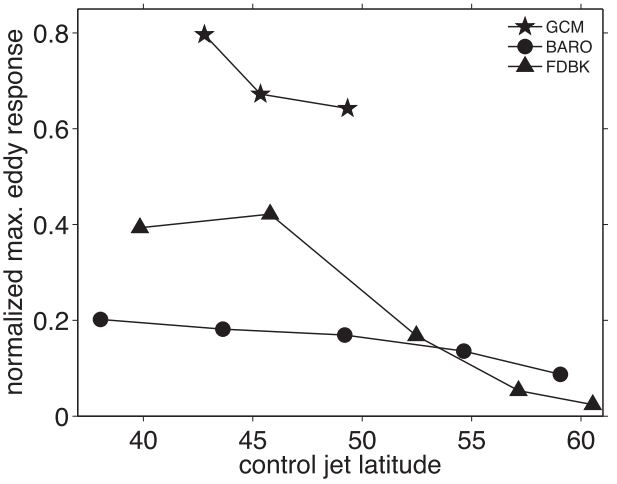

FIG. 13. Normalized maximum eddy-momentum flux convergence response poleward of the control jet irrespective of forcing latitude vs the control jet latitude for all experiments and model setups. The maxima are normalized by the maximum eddy-momentum flux convergence of the corresponding control integration.

c. Summary of mean state results

The results of this section can be summarized in Fig. 13, where we plot the normalized maximum eddy response poleward of the control jet (irrespective of the specific forcing latitude) against the latitude of the control jet. We normalize the maximum eddy response by the maximum eddy-momentum flux convergence of the corresponding control integration. For all model configurations, the relative maximum eddy response is largest when the mean jet is at lower latitudes.

6. Discussion and conclusions

In this study, we address the following question: ''Do barotropic or baroclinic eddy feedbacks dominate the atmosphere's response to a mechanical forcing?'' We present a hierarchy of barotropic model and GCM simulations where an external torque is applied over a range of latitudes and the response of the circulation is analyzed. The GCM simulations include both barotropic and baroclinic feedbacks. The barotropic model simulations are run under two configurations: the first includes only barotropic feedbacks (the BARO simulations) and the second includes both barotropic feedbacks and a parameterized baroclinic feedback (the FDBK simulations). Comparing the GCM, BARO, and FDBK simulations allows us to estimate the relative importance of baroclinic and barotropic feedbacks in the total circulation response.

The purpose of the study is thus twofold. One, it highlights a methodology for investigating the role of different eddy feedbacks in the circulation response to

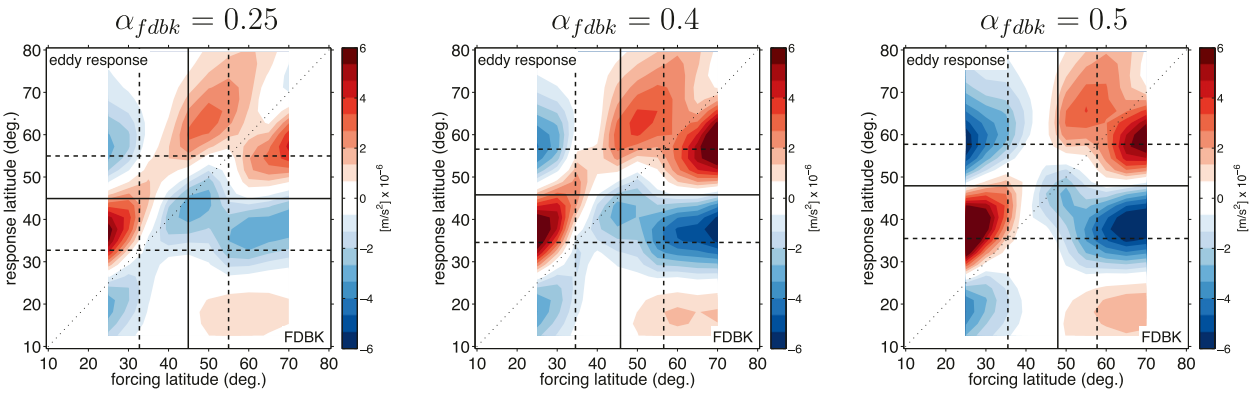

FIG. A1. Comparison of the eddy-momentum flux convergence responses for varying feedback parameters α_{fdbk} for the FDBK barotropic model experiment.

mechanical torques. Two, it investigates the relative importance of various eddy feedbacks in the circulation response to mechanical forcing.

Key findings include the following:

1) Barotropic processes are capable of capturing many aspects of the structure of the vertically integrated GCM response to an external torque, but are unable to account for the magnitude of the response.
2) Baroclinic processes appear to play a key role in setting the amplitude of the atmospheric response. The role of baroclinic processes arises through the influence of the momentum fluxes and the torque on lower-tropospheric baroclinicity and thus the location of the wave source.
3) For a given forcing, the largest response of the circulation and the eddy forcing is found poleward of the latitude of the applied torque, not at the latitude of the forcing. The maximum response of the circulation is found ~5°–10° poleward of the torque. The poleward displacement of the response is consistent with the relative effects of the climatological mean and perturbed zonal flow on the range of permitted eddy phase speeds (Fig. 6).
4) The circulation response is largest when the torque is applied approximately 10° poleward of the climatological-mean jet latitude.
5) The magnitude of the response to a torque is a function of the mean jet latitude: the response to the same torque is decreased as the climatological-mean jet latitude is increased. This effect is found in the both the barotropic model and the GCM.

These results have various implications for understanding climate variability and change; for example,

1) Observations and numerical experiments reveal that stratospheric processes have a demonstrable effect on surface climate on both month-to-month time scales (Baldwin and Dunkerton 2001) and in association with the stratospheric ozone hole (Thompson et al. 2011). The results shown here suggest that the structure of the tropospheric response is determined to first order by barotropic feedbacks at the tropopause level and that the magnitude of the response is enhanced by baroclinic feedbacks (e.g., owing to the influence of the momentum fluxes on lower-tropospheric baroclinicity; Song and Robinson 2004).
2) Climate models consistently predict a poleward shift of the jet in response to increasing greenhouse gases (e.g., Kushner et al. 2001; Miller et al. 2006; Barnes and Polvani 2013). The methodology applied here investigates the shift of the jet in numerical models with varying representations of wave–mean flow interactions. The analyses thus provide a framework for investigating the mechanisms of the shift in more complex climate models.
3) The dependence of the amplitude of the response to the mean jet latitude suggests that the sensitivity of the circulation to external forcing in the current climate may be an upper limit on the sensitivity of the circulation in future climate states. Additionally, the ubiquitous equatorward jet latitude bias among climate models (Barnes and Polvani 2013; Kidston and Gerber 2010) suggests that the current generation of climate models may overestimate the response of the circulation of the current climate to anthropogenic forcing.

Acknowledgments. EAB is funded by a NOAA Climate and Global Change Fellowship through the University Corporation of Atmospheric Research Visiting Science Program. DWJT is supported by the NSF Climate Dynamics program.

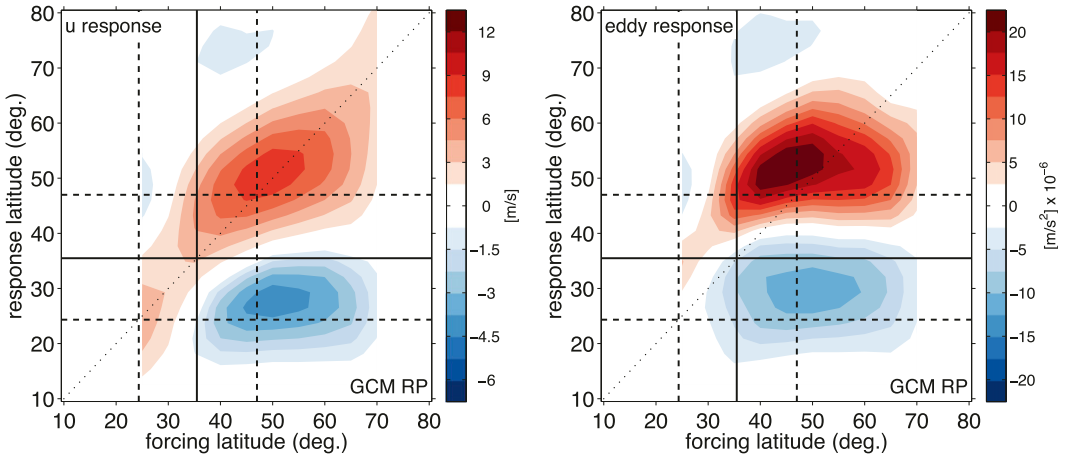

FIG. B1. As in Fig. 9, but for a run setup similar to RP07. Note the different color scale for the eddy response compared to Fig. 9.

APPENDIX A

Results for Additional Feedback Strengths

Figure A1 shows the eddy-momentum flux convergence response for $\alpha_{\text{fdbk}} = 0.25$, 0.4, and 0.5 for the FDBK barotropic model experiment. Results are qualitatively similar in all cases (after one accounts for the variations in the mean jet position), demonstrating that the main features of the eddy response are robust to small variations in the feedback between the stirring position and the flow. However, stronger feedbacks give larger responses owing to the ability of the flow to respond to the applied forcing and shift further away from θ_{fixd}.

APPENDIX B

Comparison with Ring and Plumb (2007)

Part of the motivation for this work is to extend the results of RP07, and here we briefly place their results in the context of our own. We perform an experiment identical to GCM45 but with the Rayleigh friction doubled to 0.5 days (from 1 day) to mimic the experiments performed by RP07. The only difference between this setup (denoted RP) and that of RP07 is that they introduce a hemispheric asymmetry in the equilibrium temperature profile in order to simulate austral winter. Here, we have kept the two hemispheres symmetric, but otherwise, all other parameters are identical to RP07 to the best of our knowledge.

Figure B1 shows the zonal-wind and eddy response for the RP experiment. The jet is located around 35°N, 5° south of the jet latitude in GCM43. Comparing with Fig. 9, the response of the eddies is larger in RP than the GCM43 case (note the different color scales), while the wind response is much smaller. The reduced wind response is largely due to the doubling of the drag in the simulation. The maximum jet shift for any forcing latitude in RP is 13.5° (not shown)—more than the GCM experiments discussed here. The maximum eddy response appears relatively insensitive to the forcing latitude, unlike in the simulations previously discussed (and shown in Fig. 9). The reason for the flattening of the eddy response with respect to the forcing latitude for low-latitude jets requires additional study.

REFERENCES

Baldwin, M. P., and T. J. Dunkerton, 2001: Stratospheric harbingers of anomalous weather regimes. *Science,* **294,** 581–584, doi:10.1126/science.1063315.

Barnes, E. A., and D. L. Hartmann, 2011: Rossby-wave scales, propagation, and the variability of eddy-driven jets. *J. Atmos. Sci.,* **68,** 2893–2908.

——, and C. I. Garfinkel, 2012: Barotropic impacts of surface friction on eddy kinetic energy and momentum fluxes: An alternative to the barotropic governor. *J. Atmos. Sci.,* **69,** 3028–3039.

——, and L. M. Polvani, 2013: Response of the midlatitude jets and of their variability to increased greenhouse gases in the CMIP5 models. *J. Climate,* **26,** 7117–7135.

——, D. L. Hartmann, D. M. W. Frierson, and J. Kidston, 2010: The effect of latitude on the persistence of eddy-driven jets. *Geophys. Res. Lett.,* **37,** L11804, doi:10.1029/2010GL043199.

Brayshaw, D. J., B. Hoskins, and M. Blackburn, 2008: The storm-track response to idealized SST perturbations in an aqua-planet GCM. *J. Atmos. Sci.,* **65,** 2842–2860.

Butler, A. H., D. W. J. Thompson, and T. Birner, 2011: Isentropic slopes, downgradient eddy fluxes, and the extratropical atmospheric circulation response to tropical tropospheric heating. *J. Atmos. Sci.,* **68,** 2292–2305.

Chen, G., and I. Held, 2007: Phase speed spectra and the recent poleward shift of Southern Hemisphere surface westerlies. *Geophys. Res. Lett.,* **34,** L21805, doi:10.1029/2007GL031200.

——, and P. Zurita-Gator, 2008: The tropospheric jet response to prescribed zonal forcing in an idealized atmospheric model. *J. Atmos. Sci.,* **65,** 2254–2271.

——, J. Lu, and D. M. W. Frierson, 2008: Phase speed spectra and the latitude of surface westerlies: Interannual variability and global warming trend. *J. Climate,* **21,** 5942–5959.

Chen, P., and W. A. Robinson, 1992: Propagation of planetary waves between the troposphere and stratosphere. *J. Atmos. Sci.,* **49,** 2533–2545.

Feldstein, S. B., and S. Lee, 1998: Is the atmospheric zonal index driven by an eddy feedback? *J. Atmos. Sci.,* **55,** 3077–3086.

Frierson, D. M. W., I. M. Held, and P. Zurita-Gator, 2006: A gray-radiation aquaplanet moist GCM: Static stability and eddy scale. *J. Atmos. Sci.,* **63,** 2548–2566.

Garfinkel, C. I., D. W. Waugh, and E. P. Gerber, 2013: The effect of tropospheric jet latitude on coupling between the stratospheric polar vortex and the troposphere. *J. Climate,* **26,** 2077–2095.

Gerber, E. P., and G. K. Vallis, 2007: Eddy–zonal flow interactions and the persistence of the zonal index. *J. Atmos. Sci.,* **64,** 3296–3311.

——, L. M. Polvani, and D. Ancukiewicz, 2008: Annular mode time scales in the Intergovernmental Panel on Climate Change Fourth Assessment Report models. *Geophys. Res. Lett.,* **35,** L22707, doi:10.1029/2008GL035712.

Haynes, P. H., and T. G. Shepherd, 1989: The importance of surface pressure changes in the response of the atmosphere to zonally-symmetric thermal and mechanical forcing. *Quart. J. Roy. Meteor. Soc.,* **115,** 1181–1208.

——, C. Marks, M. E. McIntyre, T. G. Shepherd, and K. P. Shine, 1991: On the ''downward control'' of extratropical diabitic circulations by eddy-induced mean zonal forces. *J. Atmos. Sci.,* **48,** 651–678.

Held, I. M., and M. J. Suarez, 1994: A proposal for the intercomparison of the dynamical cores of atmospheric general circulation models. *Bull. Amer. Meteor. Soc.,* **75,** 1825–1830.

Kidston, J., and E. Gerber, 2010: Intermodel variability of the poleward shift of the austral jet stream in the CMIP3 integrations linked to biases in the 20th century climatology. *Geophys. Res. Lett.,* **37,** L09708, doi:10.1029/2010GL042873.

——, and G. K. Vallis, 2012: The relationship between the speed and the latitude of an eddy-driven jet in a stirred barotropic model. *J. Atmos. Sci.,* **69,** 3251–3263.

Kushner, P. J., I. M. Held, and T. L. Delworth, 2001: Southern Hemisphere atmospheric circulation response to global warming. *J. Climate,* **14,** 2238–2249.

Lindzen, R. S., and B. Farrell, 1980: A simple approximate result for the maximum growth rate of baroclinic instability. *J. Atmos. Sci.,* **37,** 1648–1654.

Lorenz, D. J., and D. L. Hartmann, 2001: Eddy–zonal flow feedback in the Southern Hemisphere. *J. Atmos. Sci.,* **58,** 3312–3327.

Lu, J., G. Chen, and D. M. Frierson, 2008: Response of the zonal mean atmospheric circulation to El Niño versus global warming. *J. Climate,* **21,** 5835–5851.

——, ——, and ——, 2010: The position of the midlatitude storm track and eddy-driven westerlies in aquaplanet AGCMs. *J. Atmos. Sci.,* **67,** 3984–4000.

Miller, R. L., G. A. Schmidt, and D. T. Shindell, 2006: Forced annular variations in the 20th century Intergovernmental Panel on Climate Change Fourth Assessment Report models. *J. Geophys. Res.,* **111,** D18101, doi:10.1029/2005JD006323.

O'Gorman, P. A., 2010: Understanding the varied response of the extratropical storm tracks to climate change. *Proc. Natl. Acad. Sci. USA,* **107,** 19 176–19 180.

Ring, M. J., and R. A. Plumb, 2007: Forced annular mode patterns in a simple atmospheric general circulation model. *J. Atmos. Sci.,* **64,** 3611–3626.

Robinson, W. A., 2000: A baroclinic mechanism for the eddy feedback on the zonal index. *J. Atmos. Sci.,* **57,** 415–422.

Simpson, I. R., M. Blackburn, and J. D. Haigh, 2009: The role of eddies in driving the tropospheric response to stratospheric heating perturbations. *J. Atmos. Sci.,* **66,** 1347–1365.

——, ——, ——, and S. N. Sparrow, 2010: The impact of the state of the troposphere on the response to stratospheric heating in a simplified GCM. *J. Climate,* **23,** 6166–6185.

——, ——, and ——, 2012: A mechanism for the effect of tropospheric jet structure on the annular mode–like response to stratospheric forcing. *J. Atmos. Sci.,* **69,** 2152–2170.

Song, Y., and W. A. Robinson, 2004: Dynamical mechanisms for stratospheric influences on the troposphere. *J. Atmos. Sci.,* **61,** 1711–1725.

Thompson, D. W. J., and T. Birner, 2012: On the linkages between the tropospheric isentropic slope and eddy fluxes of heat during Northern Hemisphere winter. *J. Atmos. Sci.,* **69,** 1811–1823.

——, S. Solomon, P. J. Kushner, M. H. England, K. M. Grise, and D. J. Karoly, 2011: Signatures of the Antarctic ozone hole in Southern Hemisphere surface climate change. *Nat. Geosci.,* **4,** 741–749, doi:10.1038/ngeo1296.

Vallis, G. K., E. P. Gerber, P. J. Kushner, and B. A. Cash, 2004: A mechanism and simple dynamical model of the North Atlantic Oscillation and annular modes. *J. Atmos. Sci.,* **61,** 264–280.

Wang, S., E. P. Gerber, and L. M. Polvani, 2012: Abrupt circulation responses to tropical upper-tropospheric warming in a relatively simple stratosphere resolving AGCM. *J. Climate,* **25,** 4097–4115.

Wittman, M. A., A. J. Charlton, and L. M. Polvani, 2007: The effect of lower stratospheric shear on baroclinic instability. *J. Atmos. Sci.,* **64,** 479–496.

Yin, J. H., 2005: A consistent poleward shift of the storm tracks in simulations of 21st century climate. *Geophys. Res. Lett.,* **32,** L18701, doi:10.1029/2005GL023684.